NSRRC-J0 46>0(>014)

Macromolecules

Article

pubs.acs.org/Macromolecules

Location and Number of Selenium Atoms in Two-Dimensional Conjugated Polymers Affect Their Band-Gap Energies and Photovoltaic Performance

Jian-Ming Jiang,[†] Putikam Raghunath,[‡] Hsi-Kuei Lin,[†] Yu-Che Lin,[†] M. C. Lin,[‡,§] and Kung-Hwa Wei*[,†]

[†]Department of Materials Science and Engineering, National Chiao Tung University, 300 Hsinchu, Taiwan

[‡]Center for Interdisciplinary Molecular Science, Department of Applied Chemistry, National Chiao Tung University, 300 Hsinchu, Taiwan

[§]Department of Chemistry, Emory University, Atlanta, Georgia 30322, United States

Supporting Information

ABSTRACT: We synthesized and characterized a series of novel two-dimensional Se-atom-substituted donor (D)–π-acceptor (A) conjugated polymers—PBDTTTBO, PBDTTTBS, PBDTTSBO, PBDTSTBO, PBDTTSBS, PBDTSTBS, PBDTSSBO, and PBDTSSBS—featuring benzodithiophene (BDT) as the donor, thiophene (T) as the π-bridge, and 2,1,3-benzooxadiazole (BO) as the acceptor with different number of Se atoms at different π-conjugated locations, including the π-bridge, side chain, and electron-withdrawing units. We then systematically investigated the effect of different locations and the number of Se atoms in these two-dimensional conjugated polymers on the structural, optical, and electronics such as band-gap energies of the resulting polymers, as determined through quantum-chemical calculations, UV–vis absorption spectra, and grazing-incidence X-ray diffraction. We found that through the rational structural modification of the 2-D conjugated Se-substituted polymers the resulting PCEs could vary over 3-fold (from 2.4 to 7.6%), highlighting the importance of careful selection of appropriate chemical structures such as the location of Se atoms when designing efficient D–π-A polymers for use in solar cells. Among these tested BO-containing polymers, PBDTSTBO that has moderate band gaps and good open-circuit voltages (up to 0.86 V) when mixed with $PC_{71}BM$ (1:2, w/w) provided the highest power conversion efficiency (7.6%) in a single-junction polymer solar cell, suggesting that these polymers have potential applicability as donor materials in the bulk heterojunction polymer solar cells.

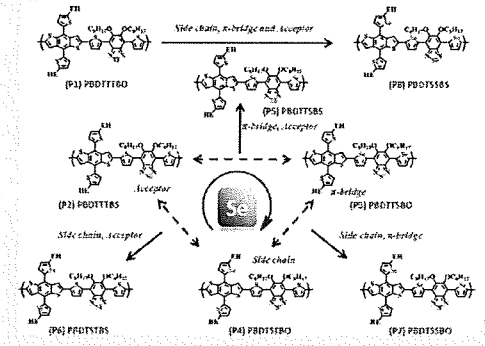

INTRODUCTION

Harvesting unlimited renewable energy from sunlight to produce electricity through photovoltaic devices is a promising means of addressing growing global energy needs while minimizing detrimental effects on the environment. Thin-film polymer solar cells (PSCs) based on bulk heterojunction (BHJ) structures, incorporating conjugated polymers possessing delocalized π electrons and fullerene derivatives, are being studied extensively because they allow the fabrication of lightweight, large-area, flexible devices using low-cost solution processing methods.[1−3] Tremendous efforts have been made toward improving the power conversion efficiencies (PCEs) of polymer BHJ devices that incorporate conjugated polymers and fullerene derivatives as their electron-donating and -accepting components, respectively.[4−8]

To obtain even higher PCEs, the search continues for optimized structures exhibiting high absorption coefficients with broad solar absorption, thereby improving the harvesting of solar light and, hence, resulting in higher short-circuit current densities (J_{sc}). Nevertheless, an improvement in PCE requires not only a greater value of J_{sc} but also suitable energy levels that are needed to ensure a high open-circuit voltage (V_{oc}) and a well-defined morphology that is needed to ensure a reasonable fill factor (FF). The ability to increase light harvesting while maintaining a deep highest occupied molecular orbital (HOMO) and high solubility remains challenging when designing new conjugated polymers as materials for polymer photovoltaic applications.[9] In attempts to harvest more photons and to tune the energy levels, several polymers have been developed featuring conjugated electron donor/acceptor (D/A) units in their main chain[10−25] or two-dimensional (2-D) conjugated configurations.[26−38] At present, the efficiencies of PSCs are now reaching beyond 10% as a result of our better understanding of the photon-to-electron conversion mechanism and the development of novel materials and tandem device architectures.[39−42]

Thiophene-containing polymers are among the materials most investigated for use in BHJ PSCs because of their π-

Received: August 21, 2014
Revised: September 17, 2014
Published: October 7, 2014

ACS Publications © 2014 American Chemical Society

conjugated character and high synthetic versatility; accordingly, an effective method to modify the optical and electronic properties of such polymers is to replace the sulfur (S) atoms within their aromatic rings with selenium (Se) atoms. Selenophene is a chalcogenophene homologue that has chemical and physical properties similar to those of thiophene; the relatively lower aromaticity of selenophene increases the ground-state quinoid resonance character of its resulting polymers, leading to improved planarity, increased effective conjugation length, and lower band-gap energy. The Se atom is much larger and less electronegative than the S atom; thus, Se-containing polymers are generally more effective at extending the absorption spectrum toward the infrared region. In addition, the Se-containing units are more polarizable than their S-containing analogues, often resulting in greater charge mobility of the polymer as a result of interchain Se···Se interactions. Indeed, Se-based conjugated polymers provide the opportunity to enhance the interchain interactions and the carrier transport phenomena because the heteroaromatic interactions of Se atoms are generally stronger than those of S atoms, favorable for applications in organic field effect transistors (OFETs).[43−45] Similarly, the conductivity and charge mobility of selenophene-based polymers are greater than those of corresponding thiophene-based polymers because of greater π-overlap resulting from the larger π-orbitals of Se atoms.[46]

Recently, it was reported that replacing the S atoms with Se atoms in the π-bridges of conjugated polymers can decrease the band-gap energy and enhance the charge transport properties in OFETs.[44,45] The photovoltaic performance of these Se-containing polymers was, however, lower than that of corresponding polymers containing thiophene π-bridges, primarily a result of higher HOMO energy levels and, thus, lower values of V_{oc} for the photovoltaic devices.[47−52] Nevertheless, a low-band-gap polymer containing selenophene π-bridges that provided a promising PCE of 7.2%, significantly higher than that (5.01%) of the corresponding polymer incorporating thiophene π-bridges, was reported.[53] Another useful Se-containing electron-deficient building block is benzoselenadiazole (BS), a benzothiadiazole (BT) analogue in which the S atom has been replaced by a Se atom.[54−57] When BS-based polymers have been used in PSCs, however, they have generally provided unsatisfactory PCEs (up to only 2.5%) because of relatively low values of V_{oc} and poorer morphologies than their corresponding BT-based polymers.[54] Nevertheless, Tajima et al. reported a low-band-gap, BS-based polymer that provided PCEs (up to 5.18%) that were slightly higher than that (5.01%) of the corresponding BT-based analogue.[58] Furthermore, some Se-substituted D−π-A copolymers in which the Se atoms were located in the side chain or in the electron-donating building block have also provided unsatisfactory PCEs.[59−62] Promising results have been obtained, however, when using selenolo[3,2-*b*]thiophene, a new electron-rich building block; its polymers have provided similar values of V_{oc} and FF and higher values of J_{sc} than those of its corresponding S-based derivatives, with the device efficiencies increasing from 5.6 to 6.8%.[63] The seemingly contradictory results detailed above suggest that there is a need to develop novel Se-based D−A-type copolymers while further investigating the effects of Se-atom substitution.

The incorporation of Se atoms into polymers decreases PCEs primarily because of higher HOMO energy levels[47−52,54−57] and limited solubility,[54,55] thereby leading to lower values of V_{oc} and less-appropriate nanomorphologies of their PCBM-blended thin films. Nevertheless, the questions remain on how and why the performances of such organic electronic devices differ so greatly. Elucidating the relationship between structure-manipulated molecular aggregates and device performance is fundamentally important for both device optimization and the structural design of new copolymers. In this study, we chose benzo[1,2-*b*:4,5-*b*′]dithiophene (BDT), a weak electron donor,[64,65] as the electron-rich unit; it is attractive for use as an electron-donating unit because of its structural symmetry and rigid fused aromatic system—features that can enhance electron delocalization and improve charge mobility.[66] To improve the solubility of polymers containing the Se-containing versions of this heterocycle, we added two alkoxy groups to the electron-deficient moieties to form benzooxadiazole (BO) as the acceptor; we also used thiophene as the π-bridge for mitigating the torsion angle between the BDT and BO units. To investigate the effect of the Se atom substitution, we synthesized eight 2-D conjugated D−π-A copolymers having different modes of Se substitution on the side chain, the π-bridge, and the electron-deficient building block. We would like to probe the effects of their structures on their absorption spectra, energy levels, hole mobility in their films, and photovoltaic performance. Morphological studies, quantum-chemical calculations, and grazing-incidence wide-angle X-ray (GIWAX) diffraction patterns have provided a greater insight into their different properties.

EXPERIMENTAL SECTION

Materials and Synthesis. 4,7-Bis(5-bromothiophen-2-yl)-5,6-bis(octyloxy)benzo[*c*][1,2,5]oxadiazole (**M1**),[67] 4,7-bis(5-bromothiophen-2-yl)-5,6-bis(octyloxy)benzo[*c*][1,2,5]selenadiazole (**M2**),[54−57] 4,7-bis(5-bromoselenophen-2-yl)-5,6-bis(octyloxy)benzo[*c*][1,2,5]-oxadiazole (**M3**),[52] 4,7-bis(5-bromoselenophen-2-yl)-5,6-bis-(octyloxy)benzo[*c*][1,2,5]selenadiazole (**M4**),[52,53] {4,8-bis[5-(2-ethylhexyl)thiophen-2-yl]benzo[1,2-*b*:4,5-*b*′]dithiophene-2,6-diyl}bis-(trimethylstannane) (**M5**),[68] and {4,8-bis[5-(2-ethylhexyl)selenophen-2-yl]benzo[1,2-*b*:4,5-*b*′]dithiophene-2,6-diyl}bis(trimethylstannane) (**M6**)[59] were prepared according to reported procedures. [6,6]-Phenyl-C_{71}-butyric acid methyl ester ($PC_{71}BM$) was purchased from Nano-C. All other reagents were used as received without further purification, unless stated otherwise. The general procedures for Stille polymerization of the either 2-D polymers are given in the Supporting Information.

^{1}H NMR spectra were recorded using a Varian UNITY 300 MHz spectrometer. Thermogravimetric analysis (TGA) was performed using a TA Instruments Q500 apparatus; the thermal stabilities of the samples were determined under a N_2 atmosphere by measuring their weight losses while heating at a rate of 20 °C min^{-1}. Size exclusion chromatography (SEC) was performed using a Waters chromatography unit interfaced with a Waters 1515 differential refractometer; polystyrene was the standard, the temperature of the system was set at 45 °C, and $CHCl_3$ was the eluent. UV−vis spectra of dilute solutions (1×10^{-5} M) of samples in dichlorobenzene (DCB) were recorded at room temperature (ca. 25 °C) using a Hitachi U-4100 spectrophotometer. Solid films for UV−vis spectroscopic analysis were obtained by spin-coating the polymer solutions onto a quartz substrate. Cyclic voltammetry (CV) of the polymer films was performed using a BAS 100 electrochemical analyzer operated at a scan rate of 50 mV s^{-1}; the solvent was anhydrous MeCN, containing 0.1 M tetrabutylammonium hexafluorophosphate ($TBAPF_6$) as the supporting electrolyte. The potentials were measured against a Ag/Ag^+ (0.01 M $AgNO_3$) reference electrode; the ferrocene/ferrocenium ion (Fc/Fc^+) pair was used as the internal standard (0.09 V). The onset potentials were determined from the intersection of two tangents drawn at the rising and background currents of the cyclic voltammograms. HOMO energy

dx.doi.org/10.1021/ma501720k | *Macromolecules* 2014, 47, 7070−7080

Scheme 1. Positions for Substitution with Se Atoms—on the Side Chains, π-Bridges, and Electron-Deficient Building Blocks—in the 2-D Conjugated Polymers

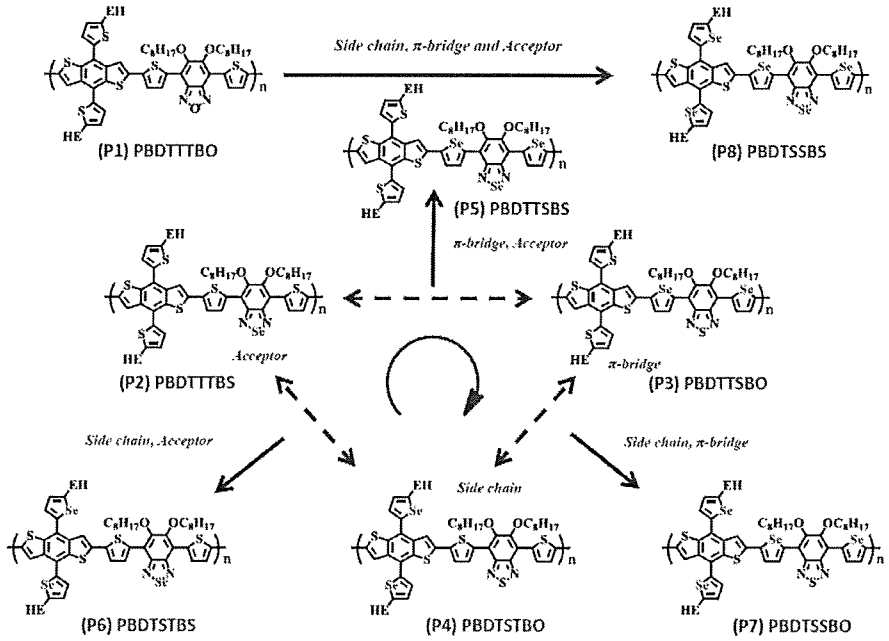

levels were estimated relative to the energy level of the ferrocene reference (4.8 eV below vacuum level). Topographic and phase images of the polymer:$PC_{71}BM$ films (surface area: 5 × 5 μm^2) were obtained using a Digital Nanoscope III atomic force microscope operated in the tapping mode under ambient conditions. The thickness of the active layer of the device was measured using a Veeco Dektak 150 surface profiler. GIWAXs experiments were performed at the National Synchrotron Radiation Research Center.

Fabrication and Characterization of Photovoltaic Devices. Indium tin oxide (ITO)-coated glass substrates were cleaned stepwise in detergent, water, acetone, and isopropyl alcohol (ultrasonication; 20 min each) and then dried in an oven for 1 h; the substrates were then treated with UV ozone for 30 min prior to use. A thin layer (ca. 20 nm) of polyethylenedioxythiophene:polystyrenesulfonate (PEDOT:PSS, Baytron P VP AI 4083) was spin-coated (5000 rpm) onto the ITO substrates. After baking at 140 °C for 20 min in air, the substrates were transferred to a N_2-filled glovebox. The polymer and PCBM were codissolved in DCB at various weight ratios, but at a fixed total concentration of 2–3 wt % (20–30 mg mL^{-1}). The blend solutions were stirred continuously for 12 h at 80 °C and then filtered through a PTFE filter (0.2 μm); the photoactive layers were obtained by spin-coating (600–2000 rpm, 60 s) the blend solutions onto the ITO/PEDOT:PSS surfaces. The thickness of each photoactive layer was approximately 90–120 nm. The devices were ready for measurement after thermal deposition (pressure: ca. 1 × 10^{-6} mbar) of a 20 nm thick film of Ca and then a 100 nm thick Al film as the cathode. The effective layer area of one cell was 0.04 cm^2. The current density–voltage (J–V) characteristics were measured using a Keithley 2400 source meter. The photocurrent was measured under simulated AM 1.5 G illumination at 100 mW cm^{-2} using a Xe-lamp-based Newport 66902 150 W solar simulator. A calibrated Si photodiode with a KG-5 filter was employed to confirm the illumination intensity. External quantum efficiencies (EQEs) were measured using an SRF50 system (Optosolar, Germany). A calibrated monosilicon diode exhibiting a response at 300–800 nm was used as a reference. For hole mobility measurements, hole-only devices were fabricated having the structure ITO/PEDOT:PSS/polymer/Au. The hole mobility was determined by fitting the dark J–V curve into the space-charge-limited current (SCLC) model,[27,69] based on the equation

$$J = \frac{9}{8}\varepsilon_0\varepsilon_r\mu_h\frac{V^2}{L^3}$$

where ε_0 is the permittivity of free space, ε_r is the dielectric constant of the polymer (assumed to be 3.0 for the conjugated polymers), μ_h is the hole mobility, V is the voltage drop across the device, and L is the thickness of the active layer.

RESULTS AND DISCUSSION

Synthesis and Characterization of Polymers. Scheme 1 outlines our design concept for the preparation of the 2-D conjugated polymers; Scheme S1 outlines our syntheses of the designed 2-D conjugated polymers. To ensure good solubility of the Se- and O-containing heterocyclic derivatives **M1**–**M4**, we positioned two neighboring octyloxy chains on the BO or BS rings, as reported previously. We synthesized **M1**,[67] **M2**,[54–57] **M3**,[52] **M4**,[52,53] **M5**,[68] and **M6**[59] using methods reported in the literature. From Stille couplings of **M1**–**M4** with **M5** and **M6** in the presence of Pd_2dba_3 as the catalyst in CB at 130 °C for 48 h, we obtained the polymers PBDTTTBO (**P1**), PBDTTTBS (**P2**), PBDTTSBO (**P3**), PBDTSTBO (**P4**), PBDTTSBS (**P5**), PBDTSTBS (**P6**), PBDTSSBO (**P7**), and PBDTSSBS (**P8**), respectively, in yields of 60–80%. Table 1 lists the number-average (M_n) and weight-average (M_w) molecular weights of these polymers, as determined through SEC, against polystyrene standards, in $CHCl_3$ as the eluent.

Physical and Thermal Stability. Table 1 summarizes the physical characteristics of all of the copolymers prepared in this study. They all exhibited high polymerization yields (60–80%) and high molecular weights (M_n = 31.2–67.3 kg mol^{-1}) after a series of Soxhlet extractions, a result of the good solubilities of the copolymers after adding the alkyl chains to both the D and A moieties. It has been reported previously that solubilizing alkyl chains can have a very significant influence on the polymerization yields and molecular weights of D–A copolymers.[70,71] Heteroatom substitution on these D–A

dx.doi.org/10.1021/ma501720k | Macromolecules 2014, 47, 7070–7080

Table 1. Molecular Weights and Thermal Properties of the Polymers

polymer	M_n[a]	M_w[a]	PDI[a]	T_d[b]
PBDTTTBO (P1)	60.2K	246.8K	4.1	334
PBDTTTBS (P2)	45.1K	157.9K	3.5	326
PBDTTSBO (P3)	56.9K	221.9K	3.9	313
PBDTSTBO (P4)	67.3K	275.9K	4.1	328
PBDTTSBS (P5)	38.7K	119.9K	3.1	315
PBDTSTBS (P6)	47.2K	160.5K	3.4	328
PBDTSSBO (P7)	52.1K	197.9K	3.8	317
PBDTSSBS (P8)	31.2K	87.4K	2.8	314

[a]Values of M_n, M_w, and PDI of the polymers were determined through GPC (in $CHCl_3$, using polystyrene standards). [b]The 5% weight-loss temperature (°C) in air.

copolymers slightly affected their polymerization yields and molecular weights, due to the same polymer backbone being shared by the S- and Se-containing copolymers. All of the copolymers had 5% weight-loss temperatures (T_d) of over 300 °C (Figure. 1), indicating their good thermal stability. In addition, copolymers having the same polymer backbone exhibited similar values of T_d. We ascribe this behavior to the thermal decomposition of the copolymers beginning at their soft parts (alkyl chains), which were identical for the same type of copolymer.

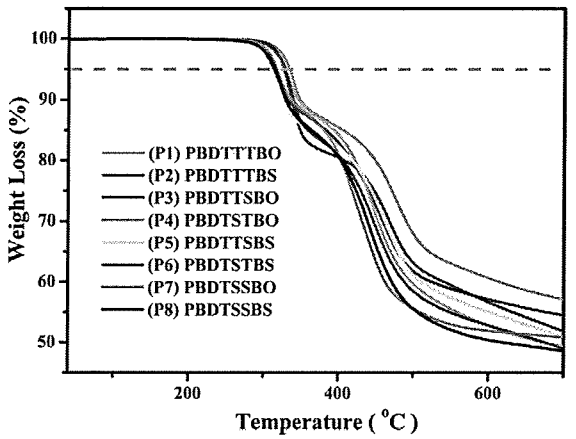

Figure 1. TGA thermograms of the copolymers P1–P8, recorded at a heating rate of 20 °C min^{-1} under a N_2 atmosphere.

Optical Properties. We recorded normalized optical UV–vis absorption spectra of dilute solutions of the polymers in DCB at room temperature and of their films spin-coated onto quartz substrates. Figure 2a displays the absorption spectra of solutions of P1–P8 in DCB at room temperature; each absorption spectrum, recorded from a dilute DCB solution, featured two absorption bands: one at 300–500 nm, which we assign to localized π–π^* transitions, and the other, a broad band from 500 to 750 nm (i.e., in the long wavelength region) corresponding to intramolecular charge transfer (ICT) between the D and A units. The absorption spectra of the eight polymers in the solid state were similar to their corresponding solution spectra, with only slight red-shifts of their absorption maxima, suggesting the presence of a few intermolecular interactions in the solid state. This behavior is in contrast to that of many conjugated polymers, in which a greater red-shift occurs upon proceeding from solution to the solid state, due to the aggregation of the polymer chains in the latter. Table 2 summarizes the optical data, including the absorption peak wavelengths ($\lambda_{max,abs}$), absorption edge wavelengths (λ_{onset}), and optical band gaps (E_g^{opt}) of the eight polymers. Notably, although the absorption profiles of the Se-substituted polymers were similar to that of the thiophene analogue, PBDTTTBO (P1), the absorption onsets of the Se-substitution polymers

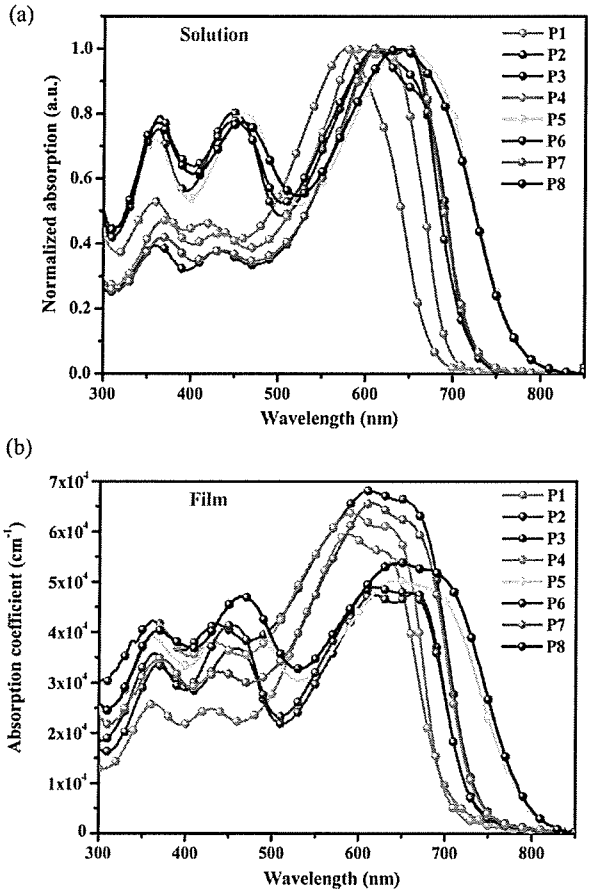

Figure 2. UV–vis absorption spectra of the polymers P1–P8 as (a) dilute solutions (1×10^{-5} M) in DCB and (b) solid films.

Table 2. Optical Properties of the Polymers

	$\lambda_{max,abs}$ (nm)		λ_{onset} (nm)	fwhm (nm)	
	solution	film	film	film	E_g^{opt} (eV)
PBDTTTBO (P1)	576	588, 626	697	163	1.78
PBDTTTBS (P2)	612	616, 664	732	176	1.69
PBDTTSBO (P3)	608, 646	610, 650	732	223	1.69
PBDTSTBO (P4)	594, 624	590, 630	697	207	1.78
PBDTTSBS (P5)	645	645	792	236	1.56
PBDTSTBS (P6)	610	618, 656	732	179	1.69
PBDTSSBO (P7)	614, 644	614, 624	732	207	1.69
PBDTSSBS (P8)	640	645	792	236	1.56

dx.doi.org/10.1021/ma501720k | Macromolecules 2014, 47, 7070–7080

Table 3. Electrochemical Properties of the Polymers

	E^{ox}_{onset} (V)	HOMO[a] (eV)	E^{opt}_g (eV)	LUMO[b] (eV)	HOMO[c] (eV)	LUMO[c] (eV)
PBDTTTBO (P1)	0.66	−5.46	1.78	−3.68	−4.82	−2.71
PBDTTTBS (P2)	0.49	−5.29	1.69	−3.60	−4.67	−2.67
PBDTTSBO (P3)	0.60	−5.40	1.69	−3.71	−4.79	−2.75
PBDTSTBO (P4)	0.66	−5.46	1.78	−3.68	−4.81	−2.72
PBDTTSBS (P5)	0.49	−5.29	1.56	−3.73	−4.65	−2.71
PBDTSTBS (P6)	0.49	−5.29	1.69	−3.60	−4.66	−2.67
PBDTSSBO (P7)	0.60	−5.40	1.69	−3.71	−4.79	−2.75
PBDTSSBS (P8)	0.49	−5.29	1.56	−3.73	−4.64	−2.71

[a]HOMO energy levels determined from the onsets of the CV curves, using the equation HOMO = $-(4.8 + E^{ox}_{onset})$ eV. [b]LUMO energy levels determined using the equation $E_{LUMO} = E_{HOMO} + E^{opt}_g$. [c]HOMO and LUMO energy levels calculated using DFT.

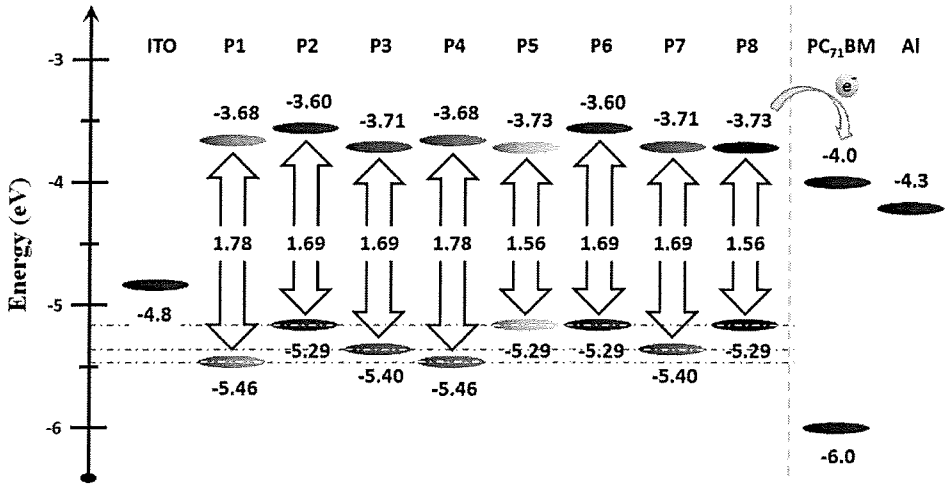

Figure 3. Energy level diagram for **P1**–**P8**.

were red-shifted significantly (by 40–100 nm). The absorption onset is red-shifted by 40 nm when Se-substitution replaced the chalcogenophene units of the 2-D conjugated polymer in a single moiety, such as the π-bridges or electron-deficient building blocks. Furthermore, when we replaced both the π-bridge and electron-deficient building block with Se atoms simultaneously, the absorption onset red-shifted by 100 nm. In contrast, modifying the side-chain groups, by changing thiophene to selenophene units, did not affect the absorption edge but did enhance the absorption coefficient (Figure. 2b). Replacing the thiophene moieties with selenophene units decreased the optical band gaps as a result of the increased quinoid character of the polymer backbone. A closer look at the film absorptions revealed that the full widths at half-maximum (FWHMs, Table 2) of the Se-substituted polymers were wider than that of PBDTTTBO (**P1**), the result of characteristic strong intermolecular Se···Se interactions, which could potentially increase the value of J_{sc} further.

Electrochemical Properties. We used CV to characterize the HOMO energy levels of the eight polymers in the form of thin films in dry MeCN containing 0.1 M Bu_4NPF_6 as the electrolyte. The cyclic voltammograms of the polymers in Figure S1 clearly indicate a partially reversible oxidation process. Table 3 lists the onset oxidation potentials (vs Ag/Ag^+) for **P1**–**P8**; from these values, we estimated the HOMO energy levels, according to the energy level of the ferrocene reference (4.8 eV below vacuum level).[72−74] Figure 3 provides the energy level diagrams of the eight polymers; we can divide the HOMO energy levels into three types. First, when we replaced the side chain group from thiophene to selenophene (e.g., **P1** ↔ **P4**, **P2** ↔ **P6**, **P3** ↔ **P7**, **P5** ↔ **P8**), the HOMO energy levels did not drift. Second, when a selenophene moiety replaced a thiophene unit in the 2-D conjugated polymer in the π-bridge, the HOMO energy level increases slightly, from −5.46 to −5.4 eV (e.g., **P3** and **P7**). Third, when the Se-containing units replaced the electron-deficient building blocks, the BS moiety dominated, increasing the HOMO energy level to −5.29 eV (e.g., **P2**, **P5**, **P6**, and **P8**). Thus, by replacing S atoms with Se atoms, the HOMO energy levels increased slightly, while those of the lowest unoccupied molecular orbitals (LUMOs) decreased slightly. The narrowing of the band gap arose mainly through the electron-stabilizing effect of the selenophene moieties because Se is a more polarizable atom than either an S or O atom.

Theoretical Calculation. We used density functional theory (DFT) to calculate the geometrical structures and absorption spectra of two repeating units (dimer-like structure) of each of the eight polymers (Scheme 1). We replaced all of the side-chain substituents (C_8H_{17} and EH) of the polymer units with CH_3 groups for computational simplification, presumably with minor effects on the electronic properties. Geometric optimization of these molecules was performed at the B3LYP/6-31G(d)[75,76] level using the Gaussian 09 simulation package,[77] with vibrational analysis undertaken at the same level to ensure no negative frequencies. Only the lowest energy conformations are reported herein. We also

dx.doi.org/10.1021/ma501720k | Macromolecules 2014, 47, 7070−7080

calculated the frontier molecular orbitals (HOMO, LUMO) at the same level of theory. We investigated the electronic nature of the absorption bands through TDDFT[78] calculations at the B3LYP/6-31G(d) level in vacuo media, up to 10 excited states.

Table S1 summarizes the main geometric parameters for the ground states in terms of various dihedral angles in the main backbones and side chains. The torsion angle θ_1 of the side chain thiophene group of the polymer PBDTTTBO was 56.8°; in its conjugated backbone, the dihedral angle θ_2 between the π-bridge thiophene and the acceptor unit of BS was 6.9°; these values suggest a high planarity of the π-conjugated systems. After Se atoms had been substituted into the BS acceptor units in the main chains, the polymers **P2** and **P6** exhibited larger values for their dihedral angles θ_2, up to 9.2°. In the case of Se substitution in both the π-bridge and the BS acceptor unit, the dihedral angles in the polymers **P5** and **P8** increased slightly (to 7.5°) relative to that (6.9°) in the unsubstituted polymer PBDTTTBO. Particularly, when we substituted Se atoms in the π-bridge on both sides of the BS units, giving the polymers **P3** and **P7**, the torsion angle decreased by 1.3° relative to **P1**. Finally, for the polymer **P4**, in which the Se atoms appeared only on the side chains, we calculated no change in the dihedral angle in the main backbone. Indeed, for all the polymers with Se atoms substituted into the side chain thiophene units, the torsion angles remained unchanged.

Next, we investigated the changes that occurred upon substituting Se atoms into various groups in the two repeating units of PBDTTTBO (**P1**) and examined the properties of the frontier orbitals; Table S2 lists the HOMO and LUMO energy levels and the HOMO–LUMO gaps (HLGs) calculated at the B3LYP/6-31G(d) level. The HOMO and LUMO energy levels of **P1** were −4.82 and −2.71 eV, respectively, giving an HLG of 2.11 eV. Substitution with Se atoms in the BS acceptor units of the π-bridges of polymers **P2**, **P5**, **P6**, and **P8** increased the energies of the HOMOs by 0.15 eV relative to that of **P1**; notably, the LUMO energy levels of polymers **P2** and **P6** increased by 0.04 eV, while those of **P5** and **P8** remained unchanged. Accordingly, the HLGs for these four polymers decreased considerably (by ca. 0.18 eV). After substituting Se atoms on both sides of the BS units in the π-bridges of the polymers **P3** and **P7**, the HOMO and LUMO energy levels increased slightly, to −4.79 and −2.75 eV, respectively. In the case of PBDTSTBO (**P4**), where Se atoms were substituted in the side-chain thiophene units, we calculated no significant changes in the HOMO and LUMO energy levels. The calculated HOMO and LUMO energy levels of all of these molecules are consistent with the experimental values in Table 3. Table S1 also displays the frontier molecular orbitals (FMOs), the HOMOs and LUMOs, of the **P1**–**P8** dimers, calculated at the B3LYP/6-31G(d) level. The calculations reveal that the molecular orbitals of the HOMO are of π nature, with electron density delocalized mainly over the whole main chain. On the other hand, the electron densities of the LUMOs are concentrated mainly on the central part of the BS acceptor unit. In both the HOMO and LUMO, the side chains contributed no electron density. The large torsion angles (>56°) between the side-chain groups and the backbone units in all of the polymers resulted in ineffective electron conjugation length over the electron-donating side chains, thereby providing similar HOMO energy levels, even though thiophene and selenophene moieties have different electron-donating abilities.

Electronic Absorption Spectra. We used quantum-chemical calculations to analyze the absorption spectra and the nature of the electronic transitions for each of the eight polymers. We calculated the electronic absorption properties using the TD-DFT method at the B3LYP/6-31G(d) level. From these calculations, we predicted (Table S2) the absorption wavelengths (λ_{abs}), oscillator strengths (f), and ground state dipole moments (μ_g) and their transitions, along with the ground-to-excited state transition dipole moments (μ_{ge}). In the case of the unsubstituted polymer PBDTTTBO (**P1**), the absorption maximum appeared near 684 nm with an oscillator strength of 2.116; its $S_0 \rightarrow S_1$ transition resulted mainly from the HOMO → LUMO transition, which contributed more than 96%. For all of the polymers, the S_2 state was contributed mainly by the H → L + 1 configuration with a low oscillator strength. The ground state dipole moments for all the molecules were less than 1.0 D. The calculated transition dipole moment (μ_{ge}) for **P1** was 16.58 D. Our results reveal that the ground-to-excited state transition dipole moments for all of these molecules, based on the Cartesian coordinate system, were oriented in the *XY*-plane, with charge transfer being dominant mainly on the *X*-axis and perpendicular to the dipole moments, lying on the backbones of the molecules. After substituting Se atoms in the BS acceptor units of **P2** and **P6** and in both the π-bridge and BS groups of **P5** and **P8**, the absorption maxima (λ_{abs}) increased by approximately 51 and 78 nm, respectively, relative to that in the unsubstituted PBDTTTBO (**P1**). These four polymers (**P2**, **P5**, **P6**, **P8**) have high torsional angles, significantly smaller oscillator strengths (ca. 1.5), and lower transition dipole moments when compared with those of **P1**. In the polymers **P3** and **P7**, the substitutions with Se atoms in the π-bridges led to increased conjugation and, thus, an increase in the absorption maxima (λ_{abs}) by 22 nm, relative to that of **P1**. These two polymers have high transition dipole moments (μ_{ge} = 18.51 D) and high oscillator strengths (ca. 2.287). According to our calculations, Se atom substitutions in the side chains of the polymer **P4** had no effect on its dihedral angles or HOMO/LUMO energy levels, but the oscillator strengths and transition dipoles did increase. The absorption maximum and oscillator strength of **P4** were 689 nm and 2.108, respectively; its transition dipole moment (μ_{ge}) was also quite large (17.55 D) along the *X*-axis of the main molecule. As a consequence, from the ground state to the vertical excited state, as the transition dipole moment (μ_{ge}) increased, the oscillator strength (f) also increased. Based on our calculations, the predicted HOMOs, LUMOs, and absorption properties of all of these polymers were consistent with the experimental data (cf. Tables 2 and 3 and Figure 3).

Hole Mobility. Figure 4 displays the hole mobilities of devices incorporating the polymer/$PC_{71}BM$ blends at a blend ratio of 1:2 (w/w). The hole mobilities, determined between the voltage drop of 0.8–1.5 V, for blends of the polymers **P1**–**P8** with $PC_{71}BM$ were 1.3×10^{-3}, 4.4×10^{-3}, 9.7×10^{-3}, 8.2×10^{-3}, 2.6×10^{-3}, 3.9×10^{-3}, 7.4×10^{-3}, and 1.7×10^{-3} $cm^2 V^{-1} s^{-1}$, respectively; Table 4 summarizes the data.

Photovoltaic Properties and Active Layer Morphology. We investigated the photovoltaic properties of the polymers in BHJ solar cells having the sandwich structure ITO/PEDOT:PSS/polymer:$PC_{71}BM$ (1:2, w/w)/Ca/Al, with the photoactive layers having been spin-coated from DCB solutions of the polymer and $PC_{71}BM$. After testing several compositions, we found that the optimized weight ratio of the polymer and $PC_{71}BM$ was 1:2.

dx.doi.org/10.1021/ma501720k | *Macromolecules* 2014, 47, 7070–7080

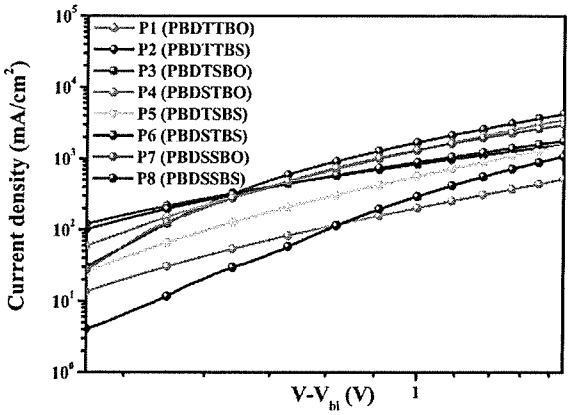

Figure 4. Dark J–V curves of hole-dominated carrier devices incorporating the polymers **P1**–**P8** blended with $PC_{71}BM$ [blend ratio, 1:2 (w/w)].

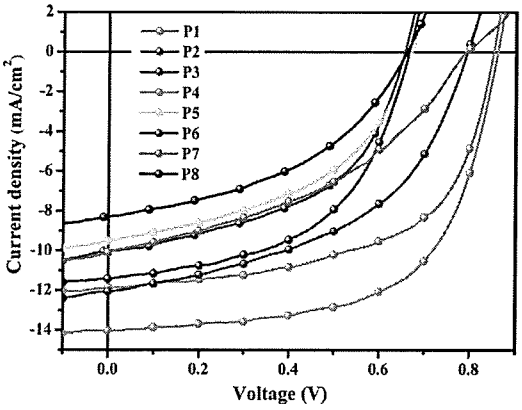

Figure 5. J–V characteristics of PSCs incorporating **P1**–**P8**/$PC_{71}BM$ blends [blend ratio, 1:2 (w/w)].

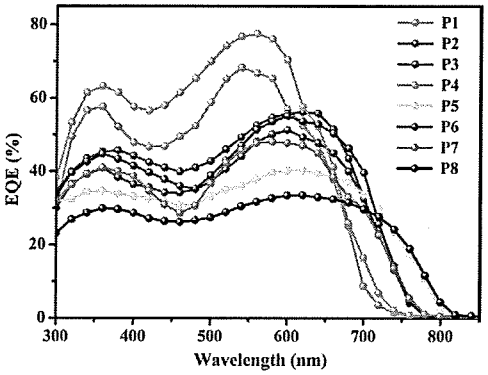

Figure 6. EQE curves of PSCs incorporating polymer:$PC_{71}BM$ blends.

Figure 5 presents the J–V curves of these PSCs; more than 10 devices were fabricated, and their average PCEs are summarizes in Table 4. The devices prepared from the blends of **P1**–**P8** with $PC_{71}BM$ exhibited open-circuit voltages (V_{oc}) of 0.85, 0.66, 0.79, 0.86, 0.67, 0.67, 0.78, and 0.66 V, respectively, corresponding to the differences between the HOMO energy levels of the polymers and the LUMO energy level of $PC_{71}BM$.[79] The short-circuit current densities (J_{sc}) of the devices incorporating blends of **P1**–**P8** and $PC_{71}BM$ were 11.8, 10.1, 11.9, 13.9, 9.5, 11.4, 10.0, and 8.3 mA cm^{-2}, respectively. Figure 6 displays the EQE curves of the devices incorporating the polymer:$PC_{71}BM$ blends at weight ratios of 1:2. The theoretical short-circuit current densities obtained from integrating the EQE curves of the **P1**–**P8** blends were 11.3, 9.9, 11.2, 13.4, 9.2, 10.9, 9.5, and 8.0 mA cm^{-2}—values that agree reasonably with the measured (AM 1.5 G) values with discrepancies of less than 5%. The highest value of J_{sc} (13.9 mA cm^{-2}) was that for the device incorporating PBDTSTBO (**P4**), presumably because of its large absorption coefficient and high hole mobility (8.2 × 10^{-3} cm^2 V^{-1} s^{-1}). Although PBDTTSBS (**P5**) and PBDTSSBS (**P8**) had, among the eight polymers, the broadest absorption ranges and FWHMs from 500 to 800 nm, their devices exhibited the lowest values of J_{sc} (9.5 and 8.3 mA cm^{-2}, respectively), presumably because of their low absorption coefficients.

The highest FF was that of the device incorporating PBDTSTBO (**P4**) in the active layer, most likely as a result of its high hole mobility. In the 2D GIWAX images of the polymer **P4** in Figure 7, we observe evidence for strong π–π stacking [d(010) = 3.63 Å] along the out-of-plane direction, indicating an isotropic structure with a slight preference for the face-on orientation. In contrast, the image for PBDTSSBS (**P8**) suggested an ordered structure with arc-shaped lamellar scattering [d(100) = 18.9 Å] and a π–π stacking [d(010) = 3.91 Å] along the out-of-plane direction, indicating both face-on and edge-on orientations. Such a face-on orientation enhances vertical charge carrier transport in PSC devices.[80−82]

When exploring the decisive factors affecting the efficiencies of PSCs, we must consider not only the absorption behavior and energy levels of the polymers but also the surface morphologies of their blends. Figure 8 displays the surface morphologies of our blend systems, determined using AFM. We prepared samples of these polymer/$PC_{71}BM$ blends using

Table 4. Photovoltaic Properties of PSCs Incorporating the Polymers

polymer/$PC_{71}BM$ (1:2)	V_{oc} (V)	J_{sc} (mA cm^{-2})	PCE_{max} ($PCE_{average}$)[a] (%)	FF (%)	mobility (cm^2 V^{-1} s^{-1})	thickness (nm)
PBDTTTBO (**P1**)	0.85	11.8	5.9 (5.76)	59	1.3 × 10^{-3}	96
PBDTTTBS (**P2**)	0.66	10.1	3.3 (3.25)	50	4.4 × 10^{-3}	95
PBDTTSBO (**P3**)	0.79	11.9	4.7 (4.61)	50	9.7 × 10^{-3}	97
PBDTSTBO (**P4**)	0.86	13.9	7.6 (7.52)	64	8.2 × 10^{-3}	104
PBDTTSBS (**P5**)	0.67	9.5	3.0 (2.87)	49	2.6 × 10^{-3}	96
PBDTSTBS (**P6**)	0.67	11.4	4.0 (3.88)	52	3.9 × 10^{-3}	109
PBDTSSBO (**P7**)	0.78	10.0	3.3 (3.26)	42	7.4 × 10^{-3}	98
PBDTSSBS (**P8**)	0.66	8.3	2.4 (2.38)	44	1.7 × 10^{-3}	105

[a]More than 10 devices were fabricated.

dx.doi.org/10.1021/ma501720k | Macromolecules 2014, 47, 7070−7080

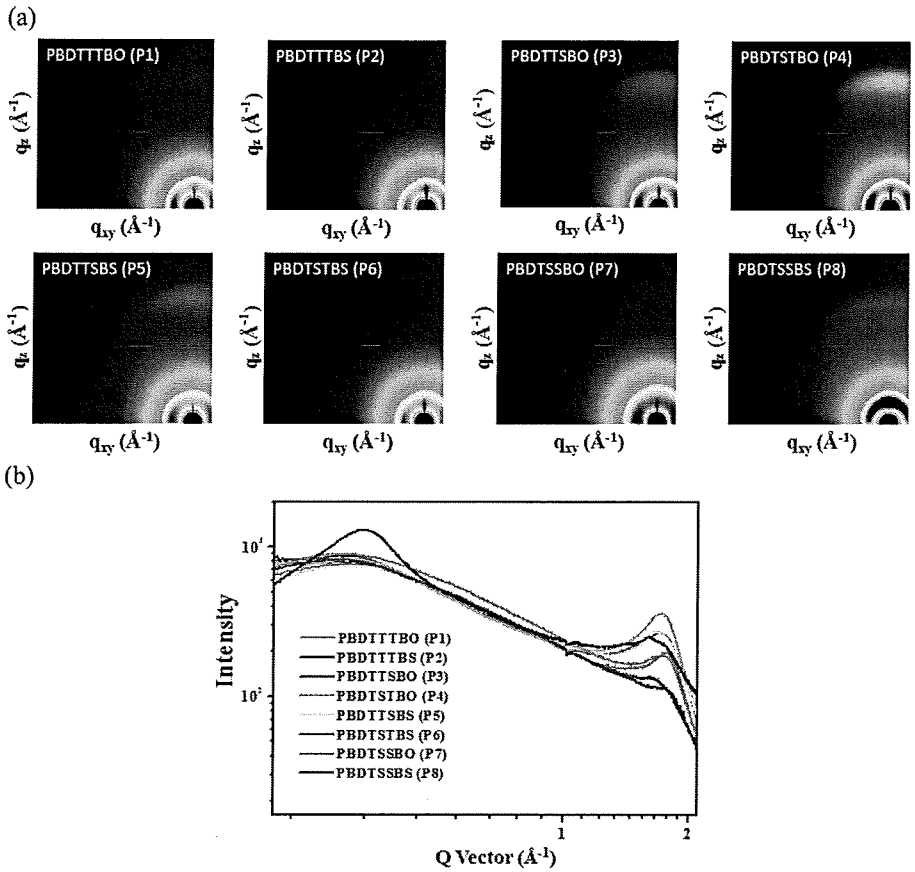

Figure 7. GIWAXS images of pure films of **P1**–**P8**: (a) 2-D images of each pure film; (b) X-ray diffraction of pure films in the out-of-plane direction.

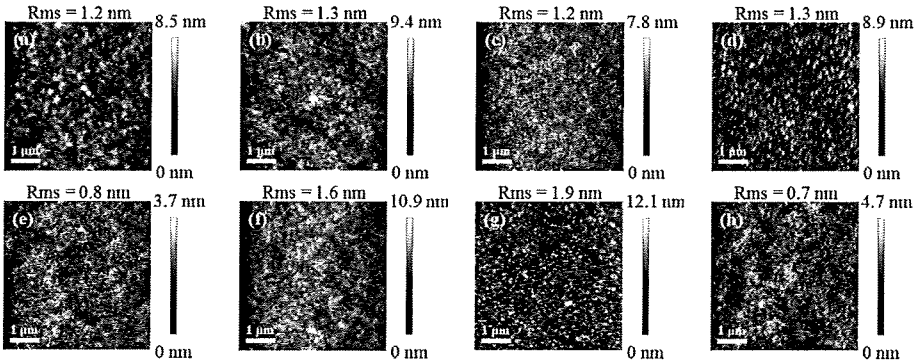

Figure 8. Topographic AFM images of polymer:$PC_{71}BM$ (1:2, w/w) blends incorporating (a) PBDTTTBO, (b) PBDTTTBS, (c) PBDTTSBO, (d) PBDSTBO, (e) PBDTTSBS, (f) PBDTSTBS, (g) PBDTSSBO, and (h) PBDTSSBS.

procedures identical to those we employed to fabricate the active layers of the devices. In each case, we observed a smooth morphology for the blends of **P1**–**P8** with $PC_{71}BM$, with root-mean-square (rms) roughnesses of 1.2, 1.3, 1.2, 1.3, 0.8, 1.6, 1.9, and 0.7 nm, respectively. Notably, the blends of PBDTTSBS (**P5**) and PBDTSSBS (**P8**) had the lowest roughnesses (0.8 and 0.7, respectively); their overly smooth morphologies might have been caused by homogeneous separation of the polymers and the fullerene. Such homogeneous blends might lead to insufficient phase separation and result in fragmented electron channels.

The effect of the molecular weight of the polymers on their photovoltaic performances depends on whether the number-average molecular weight (M_n) reaches their critical values. For some polymers that have M_n between 2 and 30 kg mol^{-1}, the PCEs of the BHJ solar cells can have large variations from 1.2 to 5.9% as reported in the literature.[83,84] When the M_n of the polymers is larger than 30 kg mol^{-1}, the effect of the molecular weight on the PCEs of the BHJ solar cells is minimized; in fact, much higher M_n results in a slight decrease in the PCEs of the BHJ solar cells such as in the case of the PTzBT-14HD polymers.[85] For understanding the effect of the molecular

dx.doi.org/10.1021/ma501720k | *Macromolecules* 2014, 47, 7070–7080

weight of our synthesized polymers on their photovoltaic devices' performances, we chose **P4**, which has the highest M_n among the molecular weights of these 2-D conjugated Se-atom-substituted polymers, for varying its molecular weight for comparing the resulting devices' photovoltaic properties. Table S3 summarizes the molecular weight characteristics of **P4** and the resulting photovoltaic devices' PCEs; Figure S2 presents the $J-V$ curves of these PSCs. The devices incorporating the blends of different molecular weight **P4** with $PC_{71}BM$ [1:2 (w/w)] exhibited an almost constant V_{oc} of 0.86 V, despite their molecular weight variations. Whereas, the J_{sc} of the devices incorporating blends of $PC_{71}BM$ and **P4** [2:1 (w/w)] with M_n of 35.6K, 51.8K, and 67.3K was 13.3, 13.4, and 13.9 mA cm^{-2}, respectively. As a result, the PCEs of photovoltaic device of **P4** with M_n of 35.6K, 51.8K, and 67.3K were 7.1, 7.4, and 7.6%, respectively, indicating that the dependence of photovoltaic properties of the devices on the molecular weight of polymer incorporated is mitigated when the number-averaged molecular weight (M_n) exceeds 50 000. Moreover, in our present study, all M_n values except two are close to or greater than 50 kg mol^{-1} (the M_n of **P1**, **P2**, **P3**, **P4**, **P5**, **P6**, P7, and **P8** was 60.2, 45.1, 56.9, 67.3, 38.7, 47.2, 52.1, and 31.2 kg mol^{-1}, respectively), and thus the effect of M_n on the PCEs is not substantial. As a result, the substitutions of the selenium atoms in these two-dimensional conjugated polymers are the main effect on their band gaps and power conversion efficiency of their BHJ solar cells.

CONCLUSION

We have synthesized eight 2-D conjugated D–π-A copolymers in which we varied the positions and the numbers of substituting Se atoms to optimize the performance of these copolymers in polymer solar cells. To explore the potential of the Se-substituted polymers as efficient active materials in solar cells, we systematically investigated the influence of the different Se-substitution patterns on the structural, optical, electrochemical, and photovoltaic properties of the polymers. Mobility measurements, morphological studies, quantum-chemical calculations, and grazing-incidence X-ray diffraction patterns have provided us with a greater insight into the different behavior of the polymers. Through rational structural modification of the 2-D conjugated Se-substituted polymers, the resulting power conversion efficiency could vary over 3-fold (from 2.4 to 7.6%), highlighting the importance of careful selection of appropriate chemical structures when designing efficient D–π-A polymers for use in solar cells. Among these polymers, the device incorporating PBDTSTBO (**P4**) exhibited the highest power conversion efficiency of 7.6%—the highest value obtained to date for a polymer containing BO moieties through a simple fabrication configuration. With its high value of V_{oc} (0.86 V) and medium band gap, the polymer **P4** appears to be a promising candidate material for use in tandem solar cells.

ASSOCIATED CONTENT

Supporting Information

General procedures for Stille polymerization of the either 2-D polymers, cyclic voltammograms, ^1H NMR spectra, simulated HOMO and LUMO electron density distributions and HOMO and LUMO energy levels, HLGs, absorption maxima, oscillator strengths, of the copolymers determined through DFT calculations, various molecular weight of **P4** and photovoltaic properties of **P4** with various M_n are show in Scheme S1, Figures S1, S2, and Tables S1, S2, S3, S4. This material is available free of charge via the Internet at http://pubs.acs.org.

AUTHOR INFORMATION

Corresponding Author

*E-mail: khwei@mail.nctu.edu.tw (K.-H.W.).

Notes

The authors declare no competing financial interest.

ACKNOWLEDGMENTS

We thank Shang-Che Lan and Chih-Ming Liu for the help in organic synthesis and X-ray characterization, respectively, and the National Science Council, Taiwan, for financial support (NSC 102-3113-P-009-002).

REFERENCES

(1) Yu, G.; Gao, J.; Hummelen, J. C.; Wudl, F.; Heeger, A. J. *Science* **1995**, *270*, 1789.
(2) Wienk, M. M.; Koon, J. M.; Verhees, W. J. H.; Knol, J.; Hummelen, J. C.; Van Hal, P. A.; Janssen, R. A. J. *Angew. Chem., Int. Ed.* **2003**, *42*, 3371.
(3) Dennler, G.; Scharber, M. C.; Brabec, C. J. *Adv. Mater.* **2009**, *21*, 1323.
(4) Su, Y. W.; Lan, S. C.; Wei, K. H. *Mater. Today* **2012**, *15*, 554.
(5) Jiang, J. M.; Yuan, M. C.; Dinakaran, K.; Hariharan, A.; Wei, K. H. *J. Mater. Chem. A* **2013**, *1*, 4415.
(6) Vandewal, K.; Himmelberger, S.; Salleo, A. *Macromolecules* **2013**, *46*, 6379.
(7) Kouijzer, S.; Michels, J. J.; Berg, M. V. D.; Gevaerts, V. S.; Turbiez, M.; Wienk, M. M.; Janssen, R. A. J. *J. Am. Chem. Soc.* **2013**, *135*, 12057.
(8) Li, Y. F. *Acc. Chem. Res.* **2012**, *45*, 723.
(9) Walker, B.; Lin, J.; Kim, C.; Welch, G. C.; Park, J. K.; Lin, J.; Zalar, P.; Proctor, C. M.; Seo, J. H.; Bazan, G. C.; Nguyen, T. Q. *Energy Environ. Sci.* **2013**, *6*, 952.
(10) Amb, C. M.; Chen, S.; Graham, K. R.; Subbiah, J.; Small, C. E.; So, F.; Reynolds, J. R. *J. Am. Chem. Soc.* **2011**, *133*, 10062.
(11) Duan, R.; Ye, L.; Guo, X.; Huang, Y.; Wang, P.; Zhang, S.; Zhang, J. P.; Hou, L.; Hou, J. H. *Macromolecules* **2012**, *45*, 3032.
(12) Huang, Y.; Guo, X.; Liu, F.; Huo, L.; Chen, Y.; Russell, T. P.; Han, C. C.; Li, Y.; Hou, J. *Adv. Mater.* **2012**, *24*, 3383.
(13) Qian, D.; Ye, L.; Zhang, M.; Liang, Y.; Li, L.; Huang, Y.; Guo, X.; Zhang, S.; Tan, Z. A.; Hou, J. *Macromolecules* **2012**, *45*, 9611.
(14) Guo, X.; Zhou, N.; Lou, S. J.; Hennek, J. W.; Ortiz, R. P.; Butler, M. R.; Boudreault, P. L. T.; Strzalka, J.; Morin, P. O.; Leclerc, M.; Navarrete, J. T. L.; Ratner, M. A.; Chen, L. X.; Chen, R. P. H.; Facchetti, A.; Marks, T. J. *J. Am. Chem. Soc.* **2012**, *134*, 18427.
(15) Xu, Y. X.; Chuen, C. C.; Yip, H. L.; Ding, F. Z.; Li, Y. X.; Li, C. Z.; Li, X.; Chen, W. C.; Jen, A. K. Y. *Adv. Mater.* **2012**, *24*, 6356.
(16) Meager, I.; Ashraf, R. S.; Rossbauer, S.; Bronstein, H.; Donaghey, J. E.; Marshall, J.; Schroeder, B. C.; Heeney, M.; Anthopoulous, T. D.; McCulloch, I. *Macromolecules* **2013**, *46*, 5961.
(17) Meager, I.; Ashraf, R. S.; Mollinger, S.; Schroeder, B. C.; Bronstein, H.; Beatrup, D.; Vezie, M. S.; Kirchartz, T.; Salleo, A.; Nelson, J.; McCulloch, I. *J. Am. Chem. Soc.* **2013**, *135*, 11537.
(18) Intemann, J. J.; Yao, K.; Yip, H. L.; Xu, Y. X.; Li, Y. X.; Liang, P. W.; Ding, F. Z.; Li, X.; Jen, A. K. Y. *Chem. Mater.* **2013**, *25*, 3188.
(19) Li, Y.; Zou, J.; Yip, H. L.; Li, C. Z.; Zhang, Y.; Chueh, C. C.; Intemann, J.; Xu, Y.; Liang, P. W.; Chen, Y.; Jen, A. K. Y. *Macromolecules* **2013**, *46*, 5497.
(20) Chen, G. Y.; Chen, Y. H.; Chou, Y. J.; Su, M. S.; Chen, C. M.; Wei, K. H. *Chem. Commun.* **2011**, *47*, 5064.
(21) Yuan, M. C.; Chiu, M. Y.; Chain, C. M.; Wei, K. H. *Macromolecules* **2010**, *43*, 6270.
(22) Bronstein, H.; Fregoso, E. C.; Hadipour, A.; Soon, Y. W.; Huang, Z.; Dimitrov, S. D.; Ashraf, R. S.; Rand, B. P.; Watkins, S. E.;

Tuladhar, P. S.; Meager, I.; Durrant, J. R.; McCulloch, I. *Adv. Funct. Mater.* **2013**, *23*, 5647.
(23) Ma, Z. F.; Sun, W.; Himmelberger, S.; Vandewal, K.; Tang, Z.; Borgqvist, J.; Scalleo, A.; Andreasen, J. W.; Inganas, O.; Andersson, M. R.; Muller, C.; Zhang, F. L.; Wang, E. *Energy Environ. Sci.* **2014**, *7*, 361.
(24) Intemann, J. J.; Yao, K.; Li, Y. X.; Yip, H. L.; Xu, Y. X.; Liang, P. W.; Chueh, C. C.; Ding, F. Z.; Yang, X.; Li, X.; Chen, Y.; Jen, A. K. Y. *Adv. Funct. Mater.* **2014**, *24*, 1465.
(25) Xu, T.; Ly, L. Y.; Zheng, T.; Szarko, J. M.; Schneider, A.; Chen, L. X.; Yu, L. P. *Adv. Funct. Mater.* **2014**, *24*, 3432.
(26) Chang, Y. T.; Hsu, S. L.; Su, M. H.; Wei, K. H. *Adv. Mater.* **2009**, *21*, 2093.
(27) Huang, F.; Chen, K. S.; Yip, H. L.; Hau, S. K.; Acton, O.; Zhang, Y.; Luo, J.; Jen, A. K. Y. *J. Am. Chem. Soc.* **2009**, *131*, 13886.
(28) Kuo, C. Y.; Huang, Y. C.; Hsion, C. Y.; Yang, Y. W.; Huang, C. I.; Rwei, S. P.; Wang, H. L.; Wang, L. *Macromolecules* **2013**, *46*, 5985.
(29) Wang, N.; Chen, Z.; Wei, W.; Jiang, Z. H. *J. Am. Chem. Soc.* **2013**, *135*, 17060.
(30) Wang, Y.; Liu, Y.; Chen, S. J.; Peng, R.; Ge, Z. Y. *Chem. Mater.* **2013**, *25*, 3196.
(31) Fang, L.; Zhou, Y.; Yao, Y. X.; Diao, Y.; Lee, W. Y.; Appleton, A. L.; Allen, R.; Reinspach, J.; Mannsfeld, S. C. B.; Bao, Z. N. *Chem. Mater.* **2013**, *25*, 4874.
(32) Liu, P.; Zhang, K.; Liu, F.; Jin, T. C.; Liu, S.; Russell, T. P.; Yip, H. L.; Huang, F.; Cao, Y. *Chem. Mater.* **2014**, *26*, 3009.
(33) Kim, J. H.; Song, C. E.; Kim, B. S.; Kang, I. N.; Shin, W. S.; Hwang, D. H. *Chem. Mater.* **2014**, *26*, 1234.
(34) Zhang, M. J.; Guo, X.; Zhang, S. Q.; Hou, J. H. *Adv. Mater.* **2014**, *26*, 1118.
(35) Guo, X.; Zhang, M. J.; Ma, W.; Ye, L.; Zhang, S. Q.; Liu, S. J.; Ade, H.; Huang, F.; Hou, J. H. *Adv. Mater.* **2014**, *26*, 4043.
(36) Cui, C. H.; Wong, W. Y.; Li, Y. F. *Energy Environ. Sci.* **2014**, *7*, 2276.
(37) Hou, J. H.; Tan, Z.; Yan, Y.; He, Y.; Yang, C. H.; Li, Y. F. *J. Am. Chem. Soc.* **2006**, *128*, 4911.
(38) Hou, L. J.; Zhang, S.; Guo, Z.; Xu, F.; Li, Y. F.; Hou, J. H. *Angew. Chem., Int. Ed.* **2011**, *50*, 9697.
(39) You, J.; Dou, L.; Yoshimura, K.; Kato, T.; Ohya, K.; Moriarty, T.; Emery, K.; Chen, C. C.; Gao, J.; Li, G.; Yang, Y. *Nat. Commun.* **2013**, *4*, 1446.
(40) You, J.; Chen, C. C.; Hong, Z.; Yoshimura, K.; Ohya, K.; Xu, R.; Ye, S.; Gao, J.; Li, G.; Yang, Y. *Adv. Mater.* **2013**, *25*, 3973.
(41) Li, K.; Li, Z.; Feng, K.; Xu, X.; Wang, L.; Peng, Q. *J. Am. Chem. Soc.* **2013**, *135*, 13549.
(42) Li, W.; Furlan, A.; Hendriks, K. H.; Wienk, M. M.; Janssen, R. A. J. *J. Am. Chem. Soc.* **2013**, *135*, 5529.
(43) Ha, J. S.; Kim, K. H.; Choi, D. H. *J. Am. Chem. Soc.* **2013**, *133*, 10364.
(44) Shashid, M.; McCarthy-Ward, T.; Labram, J.; Rossbuer, S.; Domingo, E. B.; Watkins, S. E.; Stingelin, N.; Anthopoulous, T. D.; Heeney, M. *Chem. Sci.* **2012**, *3*, 181.
(45) Kronemeijier, A. J.; Gili, E.; Schahid, M.; Pirnay, J.; Salleo, A.; Heeney, M.; Sirrighans, H. *Adv. Mater.* **2012**, *24*, 1558.
(46) Crouch, D. J.; Skabra, P. J.; Lohr, J. E.; McDouall, J. J. W.; Heeney, M.; McCulloch, I.; Sparrowe, D.; Shkunov, M.; Coles, S. J.; Horton, P. N.; Hursthouse, M. B. *Chem. Mater.* **2005**, *17*, 6567.
(47) Shahid, M.; Ashraf, R. S.; Huang, Z.; Kronemeijer, A. J.; McCarthy-Ward, T.; McCulloch, I.; Durrant, J. R.; Sirringhaus, H.; Heeney, M. *J. Mater. Chem.* **2012**, *22*, 12817.
(48) Kim, B.; Yeom, H. R.; Yun, M. H.; Kim, J. Y.; Yang, C. *Macromolecules* **2012**, *45*, 8658.
(49) Huang, J.; Zhao, Y.; He, W. W.; Jia, H.; Lu, Z. H.; Jiang, B.; Zhan, C. L.; Pei, Q.; Liu, Y. Q.; Yao, J. *Polym. Chem.* **2012**, *3*, 2832.
(50) Chen, H. Y.; Yeh, S. C.; Chen, C. T. *J. Mater. Chem.* **2012**, *22*, 21549.
(51) Alghamdi, A. A. B.; Watters, D. C.; Yi, H.; Solyman, A. F.; Almeatag, M. S.; Coles, D.; Kingsley, J.; Lidzey, D. G.; Iraqi, A. *J. Mater. Chem. A* **2013**, *1*, 5165.
(52) Rycel, L. U.; Liang, Y.; Wentao, L.; Wei, Y. *Macromolecules* **2014**, *47*, 2289.
(53) Dou, L.; Chang, W. H.; Gao, J.; Chen, C. C.; You, J. B.; Yang, Y. *Adv. Mater.* **2013**, *25*, 825.
(54) Zhao, W.; Cai, W.; Xu, R.; Yang, W.; Gong, X.; Wu, H. B.; Cao, Y. *Polymer* **2010**, *51*, 3196.
(55) Shin, S. A.; Park, J. B.; Kim, J. H.; Hwang, D. H. *Synth. Met.* **2013**, *172*, 54.
(56) Li, Y.; Pan, Z.; Miao, L.; Xing, Y.; Li, C.; Chen, Y. *Polym. Chem.* **2014**, *5*, 330.
(57) Shen, P.; Bin, H. J.; Zhang, Y.; Li, Y. F. *Polym. Chem.* **2014**, *5*, 507.
(58) Zhou, E.; Cong, J.; Hashimoto, K.; Tajima, K. *Macromolecules* **2013**, *46*, 763.
(59) Warnan, J.; Labban, A. E.; Cabanetos, C.; Hoke, E. T.; Shukla, P. K.; Risko, C.; Bredas, J. L.; McGehee, M. D.; Beaujuge, P. M. *Chem. Mater.* **2014**, *26*, 2299.
(60) Lin, H. W.; Lee, W. Y.; Lu, C.; Lin, C. J.; Wu, H. C.; Lin, Y. W.; Ahn, B.; Rho, Y.; Ree, M.; Chen, W. C. *Polym. Chem.* **2012**, *3*, 767.
(61) Lee, W. H.; Son, S. K.; Kim, K.; Lee, S. K.; Shin, W. S.; Moon, S. J.; Kang, I. N. *Macromolecules* **2012**, *45*, 1303.
(62) Chang, C. C.; Chen, C. P.; Chou, H. H.; Liao, C. Y.; Chan, S. H.; Cheng, C. H. *J. Polym. Sci., Part A: Polym. Chem.* **2013**, *51*, 4550.
(63) Saadeh, H. A.; Lu, L.; Bullock, J. E.; Wang, W.; Carsten, B.; Yu, L. P. *ACS Macro Lett.* **2012**, *1*, 361.
(64) Zhou, H.; Yang, L.; Stoneking, S.; You, W. *ACS Appl. Mater. Interfaces* **2010**, *2*, 1377.
(65) Zhang, S. Q.; Ye, L.; Zhao, W. C.; Liu, D.; Yao, H. F.; Hou, J. H. *Macromolecules* **2014**, *47*, 4653.
(66) Pan, H.; Li, Y.; Wu, Y.; Liu, P.; Ong, B. S.; Zhu, S.; Xu, G. *J. Am. Chem. Soc.* **2007**, *129*, 4112.
(67) Jiang, J. M.; Yang, P. A.; Chen, H. C.; Wei, K. H. *Chem. Commun.* **2011**, *47*, 8877.
(68) Jiang, J. M.; Lin, H. K.; Lin, Y. C.; Chen, H. C.; Lan, S. C.; Chang, C. K.; Wei, K. H. *Macromolecules* **2014**, *47*, 70.
(69) Voroshazi, E.; Vasseur, K.; Aernouts, T.; Heremans, P.; Baumann, A.; Deibel, C.; Xue, X.; Herring, A. J.; Lada, T. A.; Richter, H.; Rand, B. P. *J. Mater. Chem.* **2011**, *21*, 17345.
(70) Price, S. C.; Stuar, A. C.; You, W. *Macromolecules* **2010**, *43*, 4609.
(71) Zhou, H.; Yang, L.; Xiao, S.; Liu, S.; You, W. *Macromolecules* **2010**, *43*, 811.
(72) Zhou, E.; Wei, Q.; Yamakawa, S.; Zhang, Y.; Tajima, K.; Yang, C.; Hashimoto, K. *Macromolecules* **2010**, *43*, 821.
(73) Pommerehne, J.; Vestweber, H.; Guss, W.; Mahrt, R. F.; Bassler, H.; Porsch, M.; Daub, J. *Adv. Mater.* **1995**, *7*, 551.
(74) Liang, Y.; Feng, D.; Wu, Y.; Tsai, S. T.; Li, G.; Ray, C.; Yu, L. P. *J. Am. Chem. Soc.* **2009**, *131*, 7792.
(75) Becke, A. D. *Phys. Rev. A* **1988**, *38*, 3098.
(76) Lee, C.; Yang, W.; Parr, R. G. *Phys. Rev. B* **1988**, *37*, 785.
(77) Frisch, M. J.; Trucks, G. W.; Schlegel, H. B.; Scuseria, G. E.; Robb, M. A.; Cheeseman, J. R.; Jr. Montgomery, J. A.; Vreven, T.; Kudin, K. N.; Burant, J. C.; Millam, J. M.; Iyengar, S. S.; Tomasi, J.; Barone, V.; Mennucci, B.; Cossi, M.; Scalmani, G.; Rega, N.; Petersson, G. A.; Nakatsuji, H.; Hada, M.; Ehara, M.; Toyota, K.; Fukuda, R.; Hasegawa, J.; Ishida, M.; Nakajima, T.; Honda, Y.; Kitao, O.; Nakai, H.; Klene, M.; Li, X.; Knox, J. E.; Hratchian, H. P.; Cross, J. B.; Adamo, C.; Jaramillo, J.; Gomperts, R.; Stratmann, R. E.; Yazyev, O.; Austin, A. J.; Cammi, R.; Pomelli, C.; Ochterski, J. W.; Ayala, P. Y.; Morokuma, K.; Voth, G. A.; Salvador, P.; Dannenberg, J. J.; Zakrzewski, V. G.; Dapprich, S.; Daniels, A. D.; Strain, M. C.; Farkas, O.; Malick, D. K.; Rabuck, A. D.; Raghavachari, K.; Foresman, J. B.; Ortiz, J. V.; Cui, Q.; Baboul, A. G.; Clifford, S.; Cioslowski, J.; Stefanov, B. B.; Liu, G.; Liashenko, A.; Piskorz, P.; Komaromi, I.; Martin, R. L.; Fox, D. J.; Keith, T.; Al-Laham, M. A.; Peng, C. Y.; Nanayakkara, A.; Challacombe, M.; Gill, P. M. W.; Johnson, B.; Chen, W.; Wong, M. W.; Gonzalez, C.; Pople, J. A. *Gaussian 09, Revision C.01*; Gaussian: Wallingford, CT, 2010.
(78) Bauernschmitt, R.; Ahlrichs, R. *Chem. Phys. Lett.* **1996**, *256*, 454.

(79) Brabec, C. J.; Cravino, A.; Meissner, D.; Sariciftci, N. S.; Fromherz, T.; Rispens, M. T.; Sanchez, L.; Hummelen, J. C. *Adv. Funct. Mater.* **2001**, *11*, 374.
(80) Chen, M. S.; Niskala, J. R.; Unruh, D. A.; Chu, C. K.; Lee, O. P.; Frechet, M. J. *Chem. Mater.* **2013**, *25*, 4088.
(81) Lee, W.; Kim, G. H.; Ko, S. J.; Yum, S.; Hwang, S.; Cho, S.; Shin, Y. H.; Kim, J. Y.; Woo, H. Y. *Macromolecules* **2014**, *47*, 1604.
(82) Chiu, M. Y.; Jeng, U. S.; Liang, K. S.; Su, C. H.; Wei, K. H. *Adv. Mater.* **2008**, *20*, 2573.
(83) Coffin, R. C.; Peet, J.; Rogers, J.; Bazan, G. C. *Nat. Chem.* **2009**, *1*, 657.
(84) Tong, M.; Chu, S.; Rogers, J. T.; Schmidt, K.; Hsu, B. Y.; Moses, D.; Coffin, R. C.; Kramer, E. J.; Bazan, G. C.; Heeger, A. J. *Adv. Funct. Mater.* **2010**, *20*, 3959.
(85) Osaka, I.; Saito, M.; Mori, H.; Koganezawa, T.; Takimiya, K. *Adv. Mater.* **2012**, *24*, 425.